TUBERCULOSIS (TB) CLASSIFICATION IN CHEST RADIOGRAPHS USING DEEP CONVOLUTIONAL NEURAL NETWORKS

[1]LITON DEVNATH, [2]SUHUAI LUO, [3]PETER SUMMONS, [4]DADONG WANG

[1, 2, 3]School of Electrical Engineering and Computing, The University of Newcastle, Callaghan, NSW 2308, Australia
[4]Quantitative Imaging, CSIRO Data61, Marsfield, Sydney, NSW 2122, Australia
Email: [1]liton.devnath@uon.edu.au, [2]suhuai.luo@newcastle.edu.au, [3]peter.summons@newcastle.edu.au, [4]dadong.wang@data61.csiro.au

Abstract: Tuberculosis (TB) is a deadly disease and a major health threat in most of the low and middle income countries in the world. Chest radiography is the most common method for TB screening. The success of this type of analysis depends on the experience and interpretation skill of the radiologists who examine the chest radiographs (chest X-Rays). The development of computer-aided diagnostic (CAD) systems has accelerated the early diagnosis of TB presentations. Within the field of medical imaging in recent years, Deep Convolutional Neural Networks (CNNs) have played a vital role in segmentation techniques and feature extraction for disease detection and classification of X-rays as normal or abnormal. This paper describes the development of a simple CNN architecture, with image augmentation and X-Ray image pre-processing, to classify chest radiographs into TB positive and TB negative classes. The performance of the system is measured on three publicly available datasets: the Shenzhen chest X-ray set, the Montgomery County chest X-ray (MC) set, and the India chest X-ray set. The proposed computer-aided diagnostic system for TB screening, achieves accuracy of 87.29%, which is comparable to the performance of human radiologists.

Keywords: Deep Learning,CNNs, Tuberculosis, Chest X-Rays, Augmentation.

I. INTRODUCTION

Tuberculosis is an infectious disease caused by various strains of bacterium, usually called Mycobacterium Tuberculosis. Tuberculosis attacks the lungs, but can also affect other parts of the body through air-borne transmission. It is spread through the air by people who have an active TB infection. Some of the symptoms include coughing and sneezing, and these transmit respiratory fluids through the air. Most infections do not have symptoms and this condition is known as latent tuberculosis. About one in ten people having latent infection are untreated, and it kills more than 50% of those affected. The symptoms of active TB infection are a chronic cough with blood-tinged sputum, fever, night sweats and weight loss. This form of the disease was historically referred to as "consumption". Tuberculosis bacteria is found in different forms in three stages of TB and different symptoms are identified for these three stages. Active TB, miliary TB and latent TB are the three stages. Active TB is an illness in which the TB bacteria are rapidly multiplying and invading different organs of the body. The typical symptoms of active TB vary but include cough, phlegm, chest pain, weakness, weight loss, fever, chills and sweating at night. Multi-drug treatment is employed to treat the active form of TB. Miliary TB is a rare form of the active disease stage that occurs when TB bacteria find their way into the blood stream. In this form, the bacteria quickly spread all over the body in tiny nodules and affect multiple organs simultaneously. This form of TB can be quickly fatal. Many of those who are infected with TB do not show an overt disease; they have no symptoms and their chest x-ray may be normal. The only manifestation of this encounter may be a reaction to the tuberculin skin test (TST), or interferon-gamma release assay (IGRA). However, there is an ongoing risk that the latent infection may escalate to the active disease stage. The risk is increased by other illnesses such as HIV, or medications that may compromise the immune system. To protect against this, the United States (USA) employs a strategy of preventive therapy or treatment of latent TB infections.

This paper is organised as follows: Section 2 gives a background to the TB disease detection methods and the raw chest X-Ray (CXR) images used to detect TB. Section 3 describes the proposed modelarchitecture and the experimental method used to test it. Section 4 describes the experimental results using the proposed model on public datasets. The paper concludes in Section 5with a short discussion of the results and future work.

II. BACKGROUND OF TB DETECTION METHOD AND TB X-RAY IMAGES

2.1. Radiological Manifestations of Pulmonary Tuberculosis on Chest X-Ray Images

This following describes all findings typically associated with active pulmonary TB. A person with any of the following findings must submit sputum specimens for examination [22]:

2.1.1. Infiltrate or consolidation: If the alveoli and small airways fill with dense material, the lung is said to be consolidated. It is important to be aware that consolidation does not always mean there is infection, and the small airways may fill with material other

than pus (as in pneumonia), such as fluid, blood, or cells (cancer). They all look similar and clinical information will often help you decide the diagnosis.

2.1.2. Any cavitary lesion: Lucency (darkened area) within the lung parenchyma, with or without irregular margins that might be surrounded by an area of airspace consolidation or infiltrates, or by nodular or fibrotic (reticular) densities, or both. The walls surrounding the lucent area can be thick or thin. Calcification can exist around a cavity.

2.1.3. Nodular opacities: The chest X-ray shows bilateral multinodular opacities involving the middle and lower zones with nodules varying in size from 1-3 cm.

2.1.4. Pleural effusion: The pleura only become visible when there is an abnormality present. A pleural effusion is a collection of fluid in the pleural space. Fluid gathers in the lowest part of the chest, according to the patient's position. If the patient is upright when the X-ray is taken, then fluid will surround the lung base forming a 'meniscus' – a concave line obscuring the costophrenic angle and part or all of the hemi diaphragm. If a patient is supine, then a pleural effusion layers along the posterior aspect of the chest cavity and becomes difficult to see on a chest X-ray.

2.1.5. Hilar or mediastinal lymphadenopathy abnormalities: The hila consist of vessels, bronchi and lymph nodes. On a chest X-ray, abnormalities of these structures are represented by a change in position, size and/or density.

2.1.6. Other: Any other finding suggestive of active TB, such as miliary TB. Miliary findings are nodules of millet size (1 to 2 millimeters) distributed throughout the parenchyma.

To improve TB detection during the screening process, researchers have been developing computer-aided diagnosis (CAD) systems since the 1970s. These systems provide their diagnosis automatically and thus can be used in remote locations to aid radiologists. Initially, CAD systems consisted of four phases, namely: pre-processing, segmentation, feature extraction, and classification.
In these systems, the region-of-interest is segmented and thereafter, important features are extracted using handcrafted methods to form a feature vector. However, after the emergence of deep learning in 2012, researchers drifted away from this strategy. In deep-learning-based methods, segmentation is not necessarily required and the best features are automatically extracted using the end-to-end architecture of these methods. In this paper, we have applied a deep-learning-based method, which classifies chest X-Ray (CXR) images into classes of TB positive (TB present) and TB negative (TB absent).

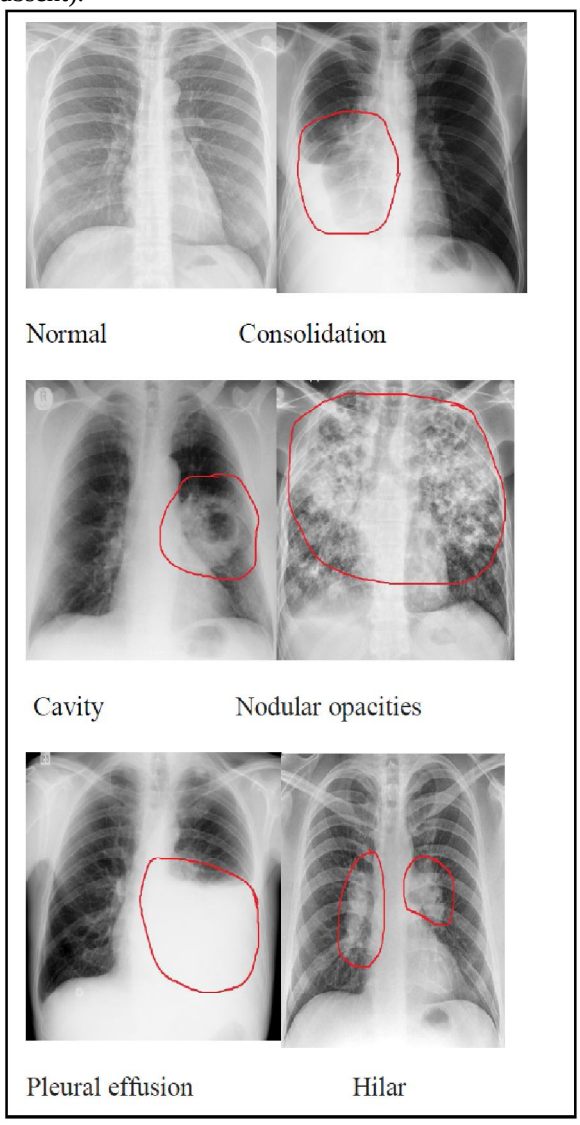

Fig.1. Radiological Manifestations of Pulmonary Tuberculosis on Chest X-Ray Images

2.2. Previous Works

Detection of TB is a challenging task due to the presence of different types of manifestations such as cavities, small opacities, large opacities, consolidation, focal lesions, and nodules on a CXR. In most of the research studies, handcrafted features are extracted and a classifier is applied to classify CXR images. For detecting specific patterns on a CXR, textural and geometrical features are most prominently used.
Jaeger et al. [1] developed an automated system that screens chest x-rays for detection of TB and other lung diseases in which an intensity mask, a lung model mask, and a Log Gabor mask are used for lungsegmentation. They extracted features for shapes, curvatures, and textures from each segmented lung field and a linear support vector machine (SVM) classifier was used to classify the CXR images into

normal and abnormal classes. The result is shown in Table1. The work of Jaeger et al. [2] proposed a similar method in which the lung boundary was extracted using graph cut segmentation method. For each segmented lung field, their system evaluated a set of features and, finally, they used a support vector machine (SVM) that classified the computed feature vectors into either normal or abnormal CXRs. Results were obtained, in which two of the datasets were used for training and one for testing the method. The results of SVM classifier is shown in Table1. The use of texture analysis in CAD has been progressively recognized [3] and Ginneken et al. [4] were the first to propose a method using local texture analysis of CXRs to detect different abnormalities. The aim of their method was to find abnormal signs of a diffuse textural nature, such as experienced in mass chest screening against tuberculosis (TB). They extracted features from histograms of the responses of a multiscale filter bank. Here, the lung fields are subdivided into several overlapping regions of various sizes and texture features are extracted for each of the regions. Divided regions are classified by voting among the k- nearest neighbours and the final classification results are combined values calculated using a weighted multiplier. Their result is shown in Table1.

Hogeweg et al. [5] presented another method that combined the multiple subsystems to detect TB in CXRs. They combined lung field and clavicle detection, textural and shape abnormality detection in their system, which improved detection performance. Here, CXRs images are divided into small circular patches and features are extracted from these patches using Gaussian derivative filters and calculated texture abnormality using a LDA (Linear Discriminant Analysis) classifier. The textural abnormality detection system, operating at the pixel level, is combined with a clavicle detection system to suppress false positive cases.

The output of a shape abnormality detection system operating at the image level is combined in a subsequent step to further improve performance by reducing false negatives. Shape abnormality is obtained by comparing the Mahalanobis distance andeither serial or parallel combinations. Their result is shown in Table1. From the clinical observations on chest radiographs shown on figure 1, it can be seen that the cavities, pleural effusion, or focal opacities, abnormalities are also the causes of TB. To detect TB cavities, Xu et al. [6] proposed a coarse-to-fine dual scale technique to detect TB cavities. In this method local cavity region-related coarse features, such as geometric, textural, and gradient features, are taken into consideration first. After that, edge-based segmentation is used for better accuracy. Finally, these contour-related features are classified using a SVM classifier to remove false positives.

Karargyris et al. [7] proposed a method to detect pulmonary and pleural abnormalities by using shape and texture features. SVM classifier is used separately on these features. Maduskar et al. [8] also proposed an algorithm to detect the pleural effusion for TB. In their method, the feature vectors are selected using angle, intensity, and morphological information, based region descriptors located around the costophrenic (CP) region. Then the normal and abnormal hemithoraces for the left/right pleural effusion are detected using a random forest classifier. Their result is shown in Table1.

Table1: Comparison of AUC (area under the curve) values with previous methods

Authors	Images	AUC (area under the curve) values
S. Jaeger et al. [1]	385	AUC:0.831
S. Jaeger et al. [2]	1000	AUC:0.90
B. Ginneken et al. [4]	388	AUC: 0.82
L. Hogeweg et al. [5]	365	AUC: 0.86
A. Karargyris et al [7]	862	AUC: 0.934
P. Maduskar et al. [8]	1267	AUC: 0.87

Recently, the research paradigm has shifted towards deep learning based methods for TB detection. The first deep convolution neural net (CNN) based method for TB detection was proposed by Hwang et al. [9] using the Alexnet network [10] and transfer learning. Chang Liu et al. [19] also used the same fine-tune deep learning networks and transfer learning. They applied shuffle sampling with cross-validation on the unbalanced dataset and the classification accuracy is shown in Table2. Cao et al. [12] also proposed deep CNN-based models to classify an image into different categories of TB manifestations. They prepared a TB dataset that includes manifestations of different TB types and modified the GoogleNet model [13] from Caffe [14] as the pre-training network (which was ImageNet [15]). They developed a new machine learning and mobile health screening system to reduce the wait-time for diagnosis. The accuracy achieved for binary classification was 89.6 %(after 100,000 iterations), whereas their accuracy for multi-class was very low at 62.07% (after 10, 0000 iterations). Rohilla et al. [16] increased the number of images and provided more variety by modifying the original images in the TB dataset [11] using image augmentation, including rotation of images to 90, 180 and 270 degrees, applying mirror images and histogram equalization. After that, they used AlexNet [10] and VGGNet [17] networks for desire classification accuracy. Hooda et al. [18] proposed a potential CNN architecture that had 7 convolutional layers and 3 fully connected layers. They compared the detection accuracy using three optimizers: namely Adam, momentum, and stochastic gradient descent (SGD) optimizers. Out of these, the Adam optimizer gave the best classification accuracy. Hooda et al. [20] also used a deep architecture named ResNet [21] for the same

classification. Here, best features are automatically extracted based on the training images and their outputs. They have also increased the dataset using data augmentation techniques.

2.3. Deep learning approaches

Deep learning, also known as deep structured learning or hierarchical learning, is part of a family of machine learning methods based on learning data representations. The idea of deep learning evolved from a biological experiment to study the visual cortex of a cat. Hubel and Wiesel, in their experiments in the 1960s, observed a rectangular topology of cells which activates in the cat's brain for a particular orientation of a drawn line. They subsequently spring up the idea of hierarchical patterns where higher details are composed of lower details. Later, Fukushima gave a new direction to this work by proposing a layered network based on unsupervised learning. LeNet[26] was one of the very first convolutional neural networks (CNNs) which helped pathway the field of Deep Learning. This guiding work was used primarily for character recognition tasks such as reading zip codes, digits, etc. Alex Krizhevsky [10] and others released AlexNet which was a deeper and much wider version of the LeNet and won by a large margin the difficult ImageNet Large Scale Visual Recognition Challenge (ILSVRC) in 2012 and significantly outperformed the second runner-up (top 5 error of 16% compared to runner-up with 26% error). AlexNet to classify the 1.2 million high-resolution images into the 1000 different classes. With AlexNet stealing the show in 2012, there was a large increase in the number of CNN models submitted to ILSVRC 2013. The winner of the competition that year was a network built by Matthew Zeiler and Rob Fergus. Named ZF Net [23], this model achieved an 11.2% error rate. An architecture known as VGG Net [17] was more of a fine tuning to the previous AlexNet structure, but still developed some very keys ideas about improving performance. Another reason this was such a great paper is that the authors spent a good amount of time explaining a lot of the intuition behind ConvNets and showing how to visualize the filters and weights correctly.Their final best network contains 16 CONV/FC layers and, appealingly, features an extremely homogeneous architecture that only performs 3x3 convolutions and 2x2 pooling from the beginning to the end. The ILSVRC 2014 winner was a ConvNets from Szegedy et al. [13] from Google. Its main contribution was the development of an Inception Module that dramatically reduced the number of parameters in the network (4M, compared to AlexNet with 60M). Additionally, this paper uses Average Pooling instead of Fully Connected layers at the top of the ConvNet, eliminating a large amount of parameters that do not seem to matter much. There are also several follow-up versions to the GoogLeNet, most recently Inception-v4. Similarly, ResNet [21] and DenseNet[24] are other popular CNN architectures which made the present era to be of deep networks.

CNN is the most commonly applied deep learning technique and is mainly used for the purpose of image classification. Convolutional operators are used to extract features from the image by sliding a filter of small size over the whole input image. In each convolution (Conv) layer, multiple filters are applied to the input image. The matrices formed by applying these filters, or kernels, are known as feature maps and are considered as the output of the convolution layer and the input to the next convolution layer. The output of each Conv layer depends on the size of filters, the number of filters, the stride of the filter, and the padding at the edges of the image. For inducing nonlinearity in the networks, a ReLu (Rectified Linear Unit) operator (such as the 'tanh' or 'sigmoid' function) is applied after each Conv layer. Most ReLu nonlinear operators then replace negative values in their feature map with zero. After some Conv steps, a pooling (max pooling or average pooling) step is performed in the network to reduce the dimension of each feature map. In max pooling, the largest element is selected using a small window (e.g. 2x2 or 3x3 etc), but in average pooling the average elements are selected without a window. Dropout layers are used for reduce overfitting the number of parameters and computations in a network. At the end of the network fully-connected dense (FC-Dense) layers are used to classify the input image into various classes using selected features from the previous networks. After the Dense layer, activation functions, such 'sigmoid' or 'softmax', are used to produce the desired classification.

III. PROPOSED CNNs ARCHITECTURE

This section describes the data and processes used for the proposed CNN architecture to classify TB classes into positive or negative.

3.1. Datasets

In this study, images from three publicly available datasets were combined to form the final dataset. These datasets included the Montgomery dataset [11], the Shenzhen dataset [11], and the India dataset [25]. The details of these datasets are summarized below:

3.1.1.Montgomery Dataset

The dataset was created by U.S. National Library of Medicine (USNLM) using the services of the health department at Montgomery County (MC), USA. It consists of 138 (58 CXRs have TB) postero-anterior (PA) CXRs collected under MC's tuberculosis screening program.The size of all of the images are 4020X4892 or 4892X4020 pixels.

3.1.2.Shenzhen Dataset

This dataset was created by USNLM in association with Guangdong Medical College, Shenzhen, China. It consists of 662 CXRs,containing 336 TB

manifested CXRs. The size of most of the images is 3000X3000 pixels.

3.1.3.India Dataset

Ground truth information is available in the form of clinical readings, annotating the abnormal locations in the CXRs. The India dataset was created by the National Institute of Tuberculosis and Respiratory Diseases, New Delhi, India. It consists of 278 CXRs, containing 125 TB manifested CXRs. The size of most of the images is 1024X2480 pixels.

3.2. Methods

The CNN models were run on a machine using the Windows operating system. The models are created using the python programming language and with the keras deep learning framework. The machine used had an Intel i5-7300U CPU@2.6-GHz processor, 8 GB of RAM, and a 64-bit operating system.

3.2.1.Preprocessing

The radiograph images in the dataset are of different size and most of the images have one color channel, i.e. grayscale, although some having three color channels, i.e. RGB. Initially, all the images are converted to RGB images, then all images are cropped to the minimum area that covers both lungs. After that resized into 1000x1000 pixels with Portable Network Graphics (PNG) format. To increase the number of images in the dataset, the method of image augmentation was used. For augmentation, the following operations were performed on the training images: they were normalized to pixel values in [0, 1], shearing and zooming transformations were randomly applied, and the images were randomly flipped.

3.2.2. Deep CNN-based method

This paper proposes a deep CNN-based method for TB detection. CNNs are based on feed-forward neural network architectures and automatic selection of features. The performance of extracted features in CNN depends on the depth of the architecture. As discussed in the previous section, CNN architecture is composed of different layers, where each layer is usually applied multiple times. It assumes that the input is in the form of 3D-images that allows the network to add certain properties.

During training, different parameter values are optimized in the Conv layers to extract meaningful features from the original input images, whereas the set of parameters to be trained in the FC layers classifies the extracted features into target classes (TB positive and TB negative in this case). Conv layers obtain visual features in a hierarchical manner from the raw input images in a way that allows lower layers to extract the low-level image features, such as edges or shapes, whereas higher layers extract the high-level visual features, e.g. parts of objects.

The proposed method uses a simple CNN architecture. The reason for using a simple architecture is that it has fewer parameters to be trained. CXR images from three different datasets, have been reduced the images 224X224 pixels in size. The images were pre-processed before use to the network. The proposed CNN architecture has 14 layers and consists of 3 Conv layers, 4 ReLu layers, 3 MaxPooling layers, 2 FC layers and 2(dropout&Flatten) layers. Conv and ReLu layers are alternatively arranged in the network. While Conv layers extract distinct features, ReLu layers are used to incorporate nonlinearity into the system. Features are extracted using random filters of 3X3 size. A different number of filters are used for different layers with no stride and zero-padding. MaxPooling layers help reduce the dimension of the feature maps. After many sets of Conv and ReLu layers, FC layers are used to resample the feature maps. They link all the features extracted by the previous layers to each neuron present in the current layer. The network uses 2 FC layers and dropout layers are sandwiched between them. Dropout layers are used to randomly disable a specific number of neurons of the previous layer, which is a commonly used regularization technique to prevent the layers from overfitting. In other words, dropout is used to decrease the influence of individual neurons, which helps the network to generalize better and also enhances accuracy. The dropout layer uses a keep probability of 0.5, which means half the neurons from the previous layer are randomly disabled.

IV. EXOPERIMENTALRESULTS

Results were evaluated by training and testing the proposed architecture on three standard available datasets. Out of total 1078 images, 768 CXRs (71%), which are randomly chosen, are used for training while remaining 310 images (29%) are used for validation purpose. The overall accuracy and validation accuracy are used as evaluation metrics. Validation accuracy is obtained by calculating the ratio of the number of correctly predicted CXRs for Tuberculosis divided by the total number of CXRs in the validation set. The overall accuracy is obtained by the ratio of the number of correctly predicted CXRs to the total number of CXRs in both the training and validation sets. The training images are divided into batches of size 32. The architecture is trained for 300 epochs, which includes 9600 steps (with a step size = training images/batch size = 24). Weights in each layer are initialized randomly using zero-mean and standard deviation of 0.01, and the initial biases are also random. To update weights after each epoch, cross entropy is used as the loss function. The overall accuracy obtained using RMSProp (for Root Mean Square Propagation) is also a method in which the learning rate is adapted for each of the parameters. The idea is to divide the learning rate for a weight by

a running average of the magnitudes of recent gradients for that weight. So, first the running average is calculated in terms of means square. The model obtained an overall training accuracy of more than 90% for the training dataset after augmentation and a validation accuracy of 87.29% for the test dataset.

Table2: Comparison of proposed CNNs model with other classification methods

Authors	Images	Accuracy
T. Xu et al. [6]	35	ACC:82.8%
Y. Cao et al. [12]	4701	ACC:89.6%(after 100,000 iterations)
A. Rohilla et al. [16]	800	ACC:80%
R. Hooda et al. [18]	800	ACC:82.09%
Chang Liu et al. [19]	4701	ACC:85.68%
R. Hooda et al. [20]	1287	ACC:84.12%
Our method	**1078**	**ACC: 77.42%(before augmentation)**
		ACC: 87.29%(after augmentation)

The performance of the proposed method is also comparable with the other methods discussed in the literature (Section 2) as shown in Table 2. The proposed model testing accuracy and loss is also shown in Fig.2-3. Before augmentation of the training data was employed, accuracy of the proposed method was low and system loss was high but after augmentation of the training data, accuracy increased to 87.29% and system loss also decreased.

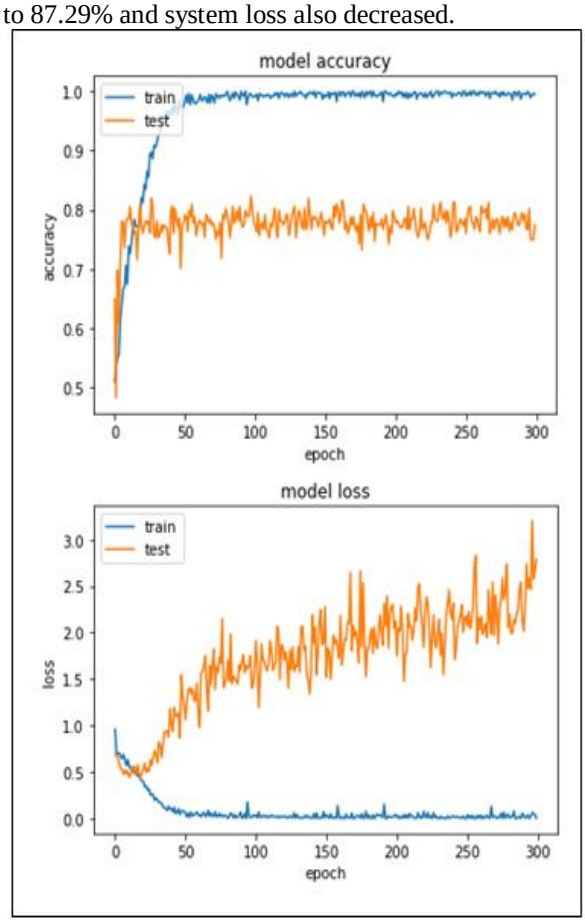

Fig.2. Overall accuracy & loss of the proposed model (before train data augmentation).

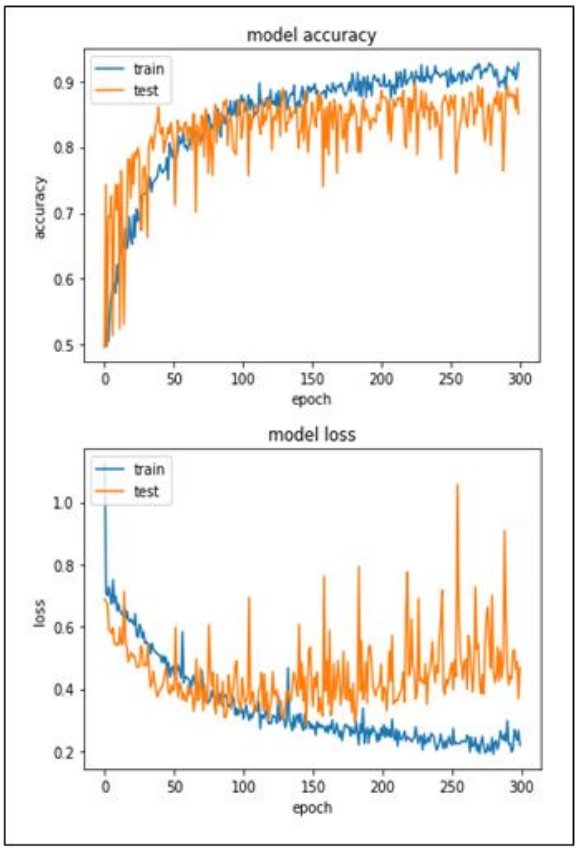

Fig.3. Overall accuracy & loss of the proposed model (after train data augmentation).

CONCLUSIONS& FUTURE WORK

This paper has proposed a TB detection method using CXRs that is based on deep CNNs. It has described its use in classifying CXR images of public datasets into TB positive and negative classes with good accuracy. The paper showed the experimental and result for the proposed method in classifying TB in--public dataset CXRs before and after training dataset image augmentation. The increase in accuracy produced by augmentation of the image data was demonstrated. The paper also provided a comparison of the performance of the proposed CNN deep leaning model with previous classification methods and architectures from the literature. Again it showed better, or comparable, accuracy to these methods.

However, for future work the proposed model needs to be tested on a bigger dataset with more variation and further verification. It is possible that in future a clinical study may be proposed to further test it validation. Another potential future work in the research will be to classify images into different TB manifestations, for which a larger dataset is also required. The effect of different types of data augmentation on the performance of the proposed architecture can also be tested. Future improvements could be evaluated in terms of using different configurations of architecture in the model and also different hardware platforms. For example, different existing standard pre-trained CNN platforms could

also be evaluated to determine the effects of transfer learning and fine-tuning, as well as different physical architecture platforms, such as a GPU or the use of High Speed Computing platforms.

ACKNOWLEDGMENTS

The work is supported by Commonwealth Scientific and Industrial Research Organisation (CSIRO) (Grant No. G1701078). We thanks to all researchers those has been provided the link of public the Montgomery dataset [11], the Shenzhen dataset [11], and the India dataset [25].

REFERENCES

[1] S. Jaeger et al., "Detecting tuberculosis in radiographs using combined lung masks", Annual International Conference of the IEEE Engineering in Medicine and Biology Society, IEEE, pp. 4978–4981, 2012.

[2] S. Jaeger et al., "Automatic tuberculosis screening using chest radiographs", IEEE transactions on medical imaging, vol. 33, no. 2, pp. 233–245, 2014.

[3] G. D. Tourassi, "Journey toward computer-aided diagnosis: Role of image texture analysis", Radiology, vol. 213, pp. 317–320, 1999.

[4] B. van Ginneken et al., "Automatic detection of abnormalities in chest radiographs using local texture analysis", IEEE transactions on medical imaging, vol. 21, no. 2, pp. 139–149, 2002.

[5] L. Hogeweg et al., "Fusion of local and global detection systems to detect tuberculosis in chest radiographs", International Conference on Medical Image Computing and Computer-Assisted Intervention, Springer, pp. 650–657, 2010.

[6] T. Xu et al., "Novel coarse-to-fine dual scale technique for tuberculosis cavity detection in chest radiographs", EURASIP Journal on Image and Video Processing, vol. 2013, no. 1, pp. 1-18, 2013.

[7] A. Karargyris et al., "Combination of texture and shape features to detect pulmonary abnormalities in digital chest x-rays", International journal of computer assisted radiology and surgery, vol. 11, no. 1, pp. 99–106, 2016.

[8] P. Maduskar et al., "Automatic detection of pleural effusion in chest radiographs", Medical image analysis, vol. 28, pp. 22–32, 2016.

[9] S. Hwang et al., "A novel approach for tuberculosis screening based on deep convolutional neural networks", SPIE Medical Imaging. International Society for Optics and Photonics, pp. 97 852W–97 852W, 2016.

[10] A. Krizhevsky et al., "Imagenet classification with deep convolutional neural networks", Advances in neural information processing systems, pp. 1097–1105, 2012.

[11] S. Jaeger et al., "Two public chest x-ray datasets for computer-aided screening of pulmonary diseases", Quantitative imaging in medicine and surgery, vol. 4, no. 6, pp. 475–477, 2014.

[12] Y. Cao et al., "Improving tuberculosis diagnostics using deep learning and mobile health technologies among resource-poor and marginalized communities", Connected Health: Applications, Systems and Engineering Technologies (CHASE), 2016 IEEE First International Conference on. IEEE, pp. 274–281, 2016.

[13] C. Szegedy et al., "Going deeper with convolutions", Proceedings of the IEEE Conference on Computer Vision and Pattern Recognition, pp. 1–9, 2015.

[14] Y. Jia et al., "Caffe: Convolutional architecture for fast feature embedding", Proceedings of the ACM International Conference on Multimedia, pp. 675-678, 2014.

[15] J. Deng et al., "Imagenet: A large-scale hierarchical image database", Computer Vision and Pattern Recognition, CVPR 2009 IEEE Conference, pp. 248-255, 2009.

[16] A. Rohilla et al., "TB Detection in Chest Radiograph Using Deep Learning Architecture", ICETETSM-17, pp. 136-147, 2017.

[17] K. Simonyan and A. Zisserman, "Very deep convolutional networks for large-scale image recognition," ICLR, pp.1-14, 2014.

[18] R. Hooda et al., "Deep-learning: A Potential Method for Tuberculosis Detection using Chest Radiography", IEEE ICSIPA, pp. 497-502, 2017.

[19] Chang Liu et al., "TX-CNN: Detecting Tuberculosis in Chest X-Ray Images Using Convolutional Neural Network", IEEE Proc. ICIP, pp.1-5, 2017.

[20] R. Hooda et al., "Automated Tuberculosis Classification of Chest Radiographs by Using Convolutional Neural Networks", IJETSR, pp.310-317, 2018.

[21] K. He et al., "Deep Residual Learning for Image Recognition", ICLR, pp. 1-12, 2015.

[22] https://www.radiologymasterclass.co.uk

[23] M. D. Zeiler et al., "Visualizing and Understanding Convolutional Networks", ICLR, 2013.

[24] G. Huang et al., "Densely Connected Convolutional Networks", ICLR, pp.1-9, 2016.

[25] R. Sivaramakrishnan et al., "Comparing deep learning models for population screening using chest radiography", Proc. of SPIE Vol. 10575 105751E-3, 2018.

[26] Y. Lecun et al., "Gradient-based Learning Applied to Document Recognition", Proc. Of IEEE, pp. 1-46, 1998.

★★★